

# The nuclear pore complex as an entropic gate: theory and simulation

Mike Castellano<sup>a</sup>, Steffen Wolf<sup>b</sup>, Thorsten Koslowski<sup>a,\*</sup>

<sup>a</sup>Institut für Physikalische Chemie, Universität Freiburg,  
Albertstraße 21, 79104 Freiburg im Breisgau, Germany

<sup>b</sup>Institut für Physik, Universität Freiburg,  
Hermann-Herder-Straße 3, 79104 Freiburg im Breisgau,  
Germany

\*Corresponding author

## Abstract

Protein chains of the  $(FG)_n$  ( $n \simeq 300$ ) type cap the cytoplasmic side of the nucleopore complex, which connects the nucleus to the remainder of an eukaryotic cell. We study the properties of three fundamental polymer models that represent these filaments using Monte Carlo computer simulations. Random walks and the worm like chain model cannot account for the unusual size selectivity of the pore, while a two-dimensional arrangement of intrinsically disordered block copolymers with a high content of  $\alpha$ -helices is in agreement with the biochemical findings. We predict a linear increase of the free energy barrier of protein transport through the pore with increasing protein diameter, which can be probed experimentally using atomic force microscopy or optical tweezers.

## 1. Introduction

In eukaryotic cells, the genetic material is located within the nucleus of the cell, which is separated from the remainder of the cell by a double membrane. This membrane is penetrated by several thousand nuclear pore complexes (NPCs), which enable the export of mRNA from the nucleus, and the import and export of proteins [1, 2, 3, 4, 5].

In figure 1, we show the structural elements of the NPC as far as relevant to our work. The part of the pore that bridges the double membrane of the nucleus has an outer diameter of  $\sim 120$  nm, the inner diameter of the pore amounts to  $\sim 52$  nm. The total height of the complex equals  $\sim 40$  nm excluding the so-called basket on the side of the nucleus, which is not shown here. On the cytoplasmatic side, the NPC is capped by eight filaments with a repetitive sequence of glycine and phenylalanine amino acids,  $(FG)_n$ , with  $\simeq 3000$  and a chain thus containing roughly 600 amino acids. The numbers given here represent the predominant variant of the human NPC, but pore dimensions or filament size can differ from organism to organism [6].

NPCs exhibit a remarkable size selectivity while importing proteins. Typically, proteins with a mass less than 4 kDa pass the membrane within seconds. With a mass of 17 kDa, the transfer may take minutes, and a mass of 40 kDa requires binding to auxiliary proteins – the appropriately named importins – to pass the pore [7]. Assuming a protein density of  $1.35$  g/cm<sup>3</sup> [8] and approximating the protein as a sphere, the molecular weights translate into diameters of 2.3, 3.4 and 4.5 nm, respectively.

Solving the structure of the individual NPC proteins and arranging them into a global model has been one of the major success stories of structural biology [9, 10]. To this success, progress in experimental cryo-transmission electron microscopy and data analysis have contributed significantly. While we can be confident that the ring and the basket parts of the pore are sufficiently rigid to be explored by the tools of structural biology, the situation is less clear for the FG filaments. Typically, in polypeptides F tends to be incorporated in  $\alpha$ -helices, and G breaks ordered secondary structures. This may introduce random orientations, resulting in chains with possible near-order structural elements, but missing a defined global structure.

The repetitive sequence of the FG filaments suggests to view them through the eyes of theoretical polymer chemistry and physics. The protein to be imported occupies a volume in space that is available to the polymer chains in its absence. Hence, the number of conformations that the polymers can explore is reduced while the protein is in reach of the chains. In turn, the entropy of the ensemble of chains is reduced, and the free energy of the system increases. This concept now has a strong experimental angle, as nanoscopic objects can be studied and manipulated using atomic force microscopy [11] or optical tweezers [12], scanning the force that is operative as a function of the distance.

From a theoretical perspective, atomistic molecular dynamics simulations can also be used to get insight into complex biochemical systems. They are limited in the size and in the time scale that can be explored, and they rely on the force field underlying the simulations. With continuous progress in simulation

algorithms and computer power, systems of the size of the NPC now lie within the range of simulations. In landmark work, Miao and Schulten have studied the components of the pore [13, 14]. They have found the arrangement of chains into a disordered brush repelling large objects entering the pore. In a large-scale effort, Ando and Gopinathan have simulated the entire yeast NPC, deriving a complex scheme for protein transport [15].

In the work presented here, we make the attempt to reduce the complexity of the system by inspecting one of its constituents, the FG filaments using coarse-grained, strongly reduced models usually at home in polymer chemistry and physics. As input, they require a very small number of parameters, which can often be obtained from conceptually simple experiments, such as small angle scattering or the measurement of elastic properties, as detailed and referenced below. In this way, we are able to verify or falsify the applicability of the models and make a statement about the structural properties of the filaments. We restrict our study to blockade effects, leaving the more complex biochemistry of importing large proteins aside in the simulations. We will, however, return to this point in the conclusions section.

In our approach, we take the configurational entropy as the only contribution to the free energy, and compute the resulting effective interaction of an idealized protein – a sphere of radius  $R_{prot}$  – with the chains. Let  $p$  be the probability of a single polymer not overlapping with the protein. We note that the probability of  $m$  filaments not overlapping with the protein amounts to  $p^m$ . We then have

$$\Delta G = -T\Delta S = -k_B T \ln p^m, \quad (1)$$

which forms the basis of our simulations. Following the model-specific rules detailed below, filaments are constructed and probed for an overlap with the protein. In turn,  $p$  and  $\Delta G$  are computed. In our model, the filaments do not interact, but their impact on gating is cumulative.

## 2. Models and methods

In the following, we present the polymer models used in this work and motivate the choice of their parameters. They are depicted schematically as short chains in figure 2. As one of the simplest polymer models, we consider the classical ideal chain or pure random walk of  $n$  monomers with an individual length  $L$ . The contour length of the polymer is given by  $\ell = nL$  (figure 2a). In two and three dimensions, the model gives rise to a scaling behaviour of the radius of gyration or the end-to-end distance as  $R_G \propto R_{ee} \propto n^{1/2}$ . Experimentally, the underlying parameters have been determined by small-angle x-ray scattering on a set of 33 denatured proteins that span a large spectrum of sequence lengths [16, 17]. With 0.598, the exponent differs little from ideal behaviour, and the average length of a monomer amounts to 1.93 Å. We note that the largest protein studied by Kohn et al. [16, 17], GroEL, contains 588 amino acids, which is close to the number of monomers in the FG filaments under review here.

In a second approach, we study the worm like chain (WLC) model in the discrete version of Kratky and Porod [18] (figure 2b). Here, two neighbouring monomers  $i$  and  $j$  experience an interaction that is proportional to the mutual

orientation of the two segments,

$$V_{ij} = -V_0 \cos \theta_{ij} \quad (2)$$

The WLC model gives rise to a squared end-to-end distance

$$R_{ee}^2 = 2P\ell \left[ 1 - \frac{P}{\ell} (1 - e^{-\ell/P}) \right] \quad (3)$$

with the thus defined persistence length  $P$  [19]. A large  $P$  is characteristic of an elastic rod-like polymer, a vanishing  $P$  recovers the ideal random walk model.  $P$  is not only related to the structural, but also to the elastic properties of the polymer. In this way, it can be determined experimentally - as for double-stranded RNA - or estimated on the basis of atomistic molecular dynamics simulations using a classical force field. For a protein  $\alpha$ -helix, Choe and Suna find  $P \simeq 100$  nm by the molecular dynamics approach [20], about twice the value of the RNA persistence length. To a large extent, this value is independent of the primary sequence of the protein. For the contour length of an  $\alpha$ -helix, we have  $\ell = n \times 1.43 \text{ \AA}$ , which leads to  $R=75$  nm for a free FG filament using eq. 3.

A large value of  $P$  implies a strong repulsive interaction between neighbouring monomers. In this regime, the potential eq. 2 can be expanded around the minimum of the potential energy at  $\theta_0 = \pi$ ,

$$V_{ij} \simeq -V_0 \left( 1 - \frac{1}{2}(\theta_{ij} - \theta_0)^2 \right). \quad (4)$$

This is tantamount to drawing the angle between two monomers from a Gaussian distribution, as we have a Boltzmann probability of finding an angle given as

$$p(\theta) = \exp\left(-\frac{V_{ij}}{k_B T}\right) \propto \exp\left(-\frac{V_0(\theta_{ij} - \theta_0)^2}{2k_B T}\right) = \exp\left(-\frac{(\theta_{ij} - \theta_0)^2}{2\sigma^2}\right) \quad (5)$$

with the variance of the Gaussian,  $\sigma = (k_B T/V_0)^{1/2}$ . As it is straightforward to generate a sequence of random numbers drawn from a Gaussian distribution [21], we follow this strategy in our simulations. The variance  $\sigma$  is calibrated to reproduce the end-to-end distance of 75 nm resulting from the WLC model, eq. 3. As described in the supporting information, we arrive at  $\sigma=2.8$  degrees. This corresponds to a  $V_0$  value of  $0.075 \text{ kcal mol}^{-1} \text{ degrees}^{-2}$ .

As a third model, we inspect a block copolymer [22] which consists of both rigid helix and random walk elements (figure 2c). We consider a FG filament as an intrinsically disordered polymer [23], where the secondary structure elements fluctuate with time or within a thermodynamic ensemble of chains. Its energy is described using a nearest-neighbour Ising-like model, where the indices  $i$  represent bonds between amino acids, which either lie within an  $\alpha$ -helix or within a random coil. We have

$$H = -J \sum_i S_i S_{i+1} \quad (6)$$

with couplings  $J$  between nearest neighbour bonds. The  $S_i$  encode the secondary structure, with  $S_i=1$  for helices and  $S_i=0$  for other structural elements. We do not consider  $\beta$ -sheets, as they only play a minor role in the secondary structure, as suggested by the Robetta structure predictions described below.  $J$  is positive, and thus the formation of helices is favoured. Monomer lengths are  $1.43 \text{ \AA}$  for helices and  $1.93 \text{ \AA}$  otherwise, in accord with the models described above. For large values of  $J^* = J/k_B T$ , this model essentially becomes a defect model, where long helices are changing their orientation at junctions defined by the defects. We are aware of the more complex nature of the chemical bond within  $\alpha$ -helices, which is mediated by

a strong non-covalent hydrogen bond between 1-4 (or third-nearest) neighbours. Nevertheless, we are confident that on the large length scale of some ten nanometers, a coarse-grained model is applicable.

All of the three polymer models are simulated by Monte Carlo procedures. Initially, the head of the polymer chain is placed on the circle that defines the pore, and the polymer is built by adding monomers consecutively. For the ideal chain, the monomer  $i + 1$  is randomly placed on a circle (2d model) or sphere (3d model) of a radius  $L$  centered at the position of the  $i$ 'th monomer. For the Kratky-Porod model, a sequence of inter-monomer angles is generated, which forms the input of a standard structure builder based on the TINKER molecular modeling package. Dihedral angles are drawn from a binary distribution (zero or 180 degrees) within the 2d model, or from a uniform distribution of angles in 3d.

The construction of the block copolymer model is performed in two steps. First, the secondary structure is simulated using the Ising-like model, equ. 6. From this simulation, statistically independent snapshots are taken. Based on these snapshots, the geometry is constructed as either adding a monomer in a random direction ( $S_i = 0$ ), or by prolonging a rigid linear chain ( $S_i = 1$ ).

### **3. Results and discussion**

In our simulations, all filament models have been grafted to the interior of the cytoplasmatic ring. Continuous random walks (CRWs) in two and three dimensions have been simulated using  $10^6$  realizations, of which at

least several thousand do not overlap with the membrane or pore wall in two dimensions. In three dimensions, we typically find  $10^4$  realizations that neither overlap with the membrane nor collide with the walls of the pore. Only the conformations not overlapping with the membrane or protein wall have been considered for the computation of the free energy according to eq. 1. The domains of overlap lie outside a circle in two dimensions, and outside a cylinder and within the membrane in three dimensions. The sphere representing the protein is always centered in the pore. It is located at the entry of the cytoplasmic side of the pore where  $p$ , the probability of not overlapping with the sphere, becomes a minimum. The geometry is illustrated in figure 3.

For random walk models of the  $(FG)_n$  polypeptide, the computed free energy, eq. 1, is shown in figure 4 as a function of the radius of the sphere. It is virtually zero for a protein radius smaller than 14 nm, and it rises steeply at a larger radius. We find a barrier height equal to the thermal energy  $k_B T$  at  $\sim 18$  nm in two dimensions, which is shifted towards  $\sim 21$  nm in three dimensions. The continuous random walks do not show any size-dependent selectivity effects below 12 nm and hence can be ruled out as models of the FG filament structure. These findings can be easily rationalized, as free random walks that are described by the model parameters used here exhibit an end-to-end distance of  $R_{ee} = \sqrt{n}L = \sqrt{600} \times 1.43\text{\AA} = 3.5$  nm. This value cannot be expected to increase by orders of magnitude while slightly constraining the configuration space. Hence, entropic repulsion by CRWs becomes operative at a length scale of  $R_{pore} - R_{ee} \simeq 20$  nm.

For  $2 \times 10^6$  realizations of the two-dimensional Kratky-Porod model, we find a very small fraction of filament realizations ( $\sim 1000$ ) that do not show overlap with the membrane or the wall of the pore. This behaviour can be easily rationalized inspecting the average end-to-end distance of the corresponding free chain,  $R_{ee} = 75$  nm, which is slightly larger than the pore diameter of 52 nm. Nonetheless, the barrier for protein transport is not very steep for this model, and we reach  $\Delta G = k_B T$  at  $R_{prot} = 15$  nm. The situation is different for the three-dimensional Kratky-Porod model (KPM), where the fraction of chains not overlapping with the membrane or the wall of the pore is comparable to that of the CRW models. Overlap even with large model proteins is, however, small. The corresponding barrier is always smaller than  $k_B T$  even for protein radii very close to the pore radius, cf. fig. 4.

The properties of the two-dimensional block copolymer model depend on the dimensionless coupling parameter,  $J^*$ . A reasonable choice for  $J^*$  would be the free energy content of the formation of a hydrogen bond between two amide groups in water, which has been found in a range of ca.  $2-8 k_B T$  [24, 25]. For a moderate  $J^* = 1.0$ , the barrier steeply increases with an increasing protein radius. The barrier is considerably higher than that of the continuous random walks and the three-dimensional Kratky-Porod model. It is, however, considerably smaller than  $k_B T$  in the range of radii where the size selectivity is operative, i.e. between 1.1 and 2.4 nm. It can be shifted into that range by increasing  $J^*$  to 2.2, corresponding to the lower end of amide hydrogen bond free energies. Here, we find a barrier that is with increasing protein radius, and we have  $\Delta G = k_B T$  at  $R_{prot} \simeq 1$  nm, a barrier that can be easily passed thermally.

Relative errors of the simulation methods have been evaluated at free energy barriers of  $k_B T$  by simulating 50 realizations using the same parameters and number of Monte Carlo steps as in the production runs. Via the root mean square variations, we find relative errors of 0.04 (continuous random walk, 2d), 0.03 (continuous random walk, 3d), 0.08 (Kratky-Porod model in 2d, block copolymer with  $J^*=2.2$ ) and 0.11 (Kratky-Porod model in 2d, block copolymer with  $J^*=1.0$ ). For the three-dimensional Kratky-Porod model, this quantity has been computed as 0.03 at a barrier height of  $k_B T/2$ .

In addition to the Monte Carlo simulations, we have inspected (FG)<sub>20</sub> oligomers from a bioinformatics angle. We have used the Robetta suite, which combines homology modelling and a *de novo* fragment insertion method [26]. The results of five predicted structural models are presented in figure 5 and in table 1. The assignment of the secondary structure elements has been made with the help of the 2Struc program [27]. This analysis is largely heuristic and is to be viewed with some caution. Nevertheless, it provides additional information on the structure of the FG filaments. All but one model predict a mixture of  $\alpha$ -helical and random secondary structure elements, with the exception of one model that finds a small contribution of  $\beta$ -sheets.

## 4. Conclusions

To get insight into the nature of the gating mechanism of the nuclear pore complex, we have inspected simple models of polymer science to describe the FG filaments capping the complex. Their space of conformations is restricted

by a spherical model protein passing the pore, giving rise to an entropic barrier. The systems have been simulated by Monte Carlo methods. The models are checked qualitatively against the peculiar size selectivity of the pore. The selectivity sets in at protein diameters in the range of 3-5 nm, values that are considerably smaller than the pore diameter of 52 nm. In the range of interest, continuous random walk models and the Kratky-Porod model lead to barriers that are much smaller than  $k_B T$  and can hence be easily overcome by diffusion. This statement holds both for two- and three-dimensional variants of the models.

On the other hand, a two-dimensional block copolymer model of the filaments shows promising features interacting with comparatively small proteins. It predominately consists of rigid  $\alpha$ -helices that are linked by disordered structural elements. In the model, the disorder induces a reorientation of the protein, cf. figure 2. In the parameter range of interest, it is reduced to a handful of defects ( $\sim 1-2\%$ ) that break the helix and its orientation. With increasing protein diameter, the free energy barrier increases linearly. It equals  $k_B T$  at a small length scale of  $R_{prot} \sim 0.75$  nm. This does not rule out the applicability of polymer models not tested. In particular, in two dimensions different models may show a very similar scaling behaviour [28].

The structural elements of block copolymer model also dominate homology models of short FG oligomers, albeit with a different weight. Experimental structures of the proteins mediating protein transport through the pores, the importins, are available [29, 30]. It is interesting to note they also contain FG repeats with a high content of  $\alpha$ -helices. Given our findings, it might be

the role of importins to locally stabilize defects in the block copolymer, thus locally lowering  $J^*$  and the energetical barrier for diffusion through the NPC.

Our interpretation of the block copolymers is a dynamic one. The defect positions change with time, and in a thermodynamic ensemble many different realizations will coexist. From this perspective, the FG filaments can also be viewed as intrinsically disordered proteins. In the limit of a defect model, the probability distribution of finding a helix of a certain length among the amino acids of the filament is a long-tailed one, cf. the supporting information. Under these conditions, a random walk consisting of large rigid helices explores space much more efficiently than a standard random walk with equal step size. For the FG filaments, this is tantamount to a very efficient blockade of the pore. Such a process has been referred to as a Levy flight by Mandelbrot [31].

From our perspective, the gating function of the nucleopore FG filaments provides a rare example in protein biochemistry: here, the function of a protein is not based on the specific chemistry of an elaborate sequence of amino acids fine-tuned by evolution, but on a simple, repetitive pattern that mainly works according to the laws of polymer physics.

## **Acknowledgements**

It is a pleasure to thank T. Friedrich, T. Hugel, K. Jahnke, J. Kaiser and N. Kremer for fruitful discussions

## **Data Availability Statement**

The data that support the findings of this study are available from the corresponding author upon reasonable request.

**Table 1**

Secondary structure analysis of homology models of (FG)<sub>20</sub> oligomers, as predicted by the Robetta suite [26].

model	1	2	3	4	5
helix	63	20	26	34	57
sheet	0	14	0	0	0
other	37	66	74	66	43

## Figure captions

### Figure 1

Model of the nuclear pore complex showing the constituents relevant to our work. a. FG filaments, b. cytoplasmatic ring, c. central framework, d. nuclear ring, e. top view.

### Figure 2

Short sequences of polymer models used in this work. a. continuous random walk, b. the Kratky-Porod model as the discrete version of the worm like chain model and c. block copolymer model.

### Figure 3

Illustration of acceptance and rejection within the two-dimensional Monte Carlo simulations. a. membrane and nuclear pore complex wall, b. pore, c. protein, d. accepted polymer conformation, e. rejected polymer conformation (collision with protein), f. polymer conformation discarded due to collision with the membrane or wall of the nuclear pore complex.

### Figure 4

Free energy barriers for the transfer of hard spheres as a function of their radius. The symbols correspond to the following polymer models: block copolymer, 2d,  $J^*=2.2$  ( $\circ$ ), block copolymer, 2d,  $J^*=1.0$  ( $\nabla$ ), block copolymer, 3d,  $J^*=2.2$  ( $\triangle$ ), continuous random walk, 2d (+), continuous random walk, 3d

( $\times$ ), Kratky-Porod model, 2d ( $\bullet$ ) and the Kratky-Porod model in 3d ( $\square$ ).

**Figure 5**

Five models of secondary structure for  $(FG)_{18}$ , as suggested by the Robetta program package [26] and analyzed using the DSSP approach [27]. In the color version of the image,  $\alpha$ -helices are drawn in red,  $\beta$ -sheets are colored yellow, and others are depicted in green.

Figure 1

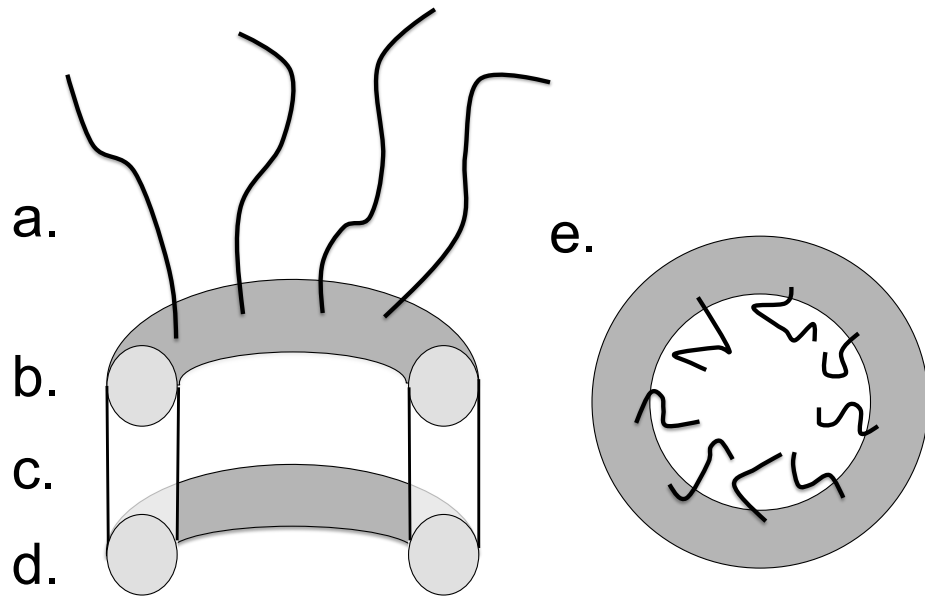


Figure 2

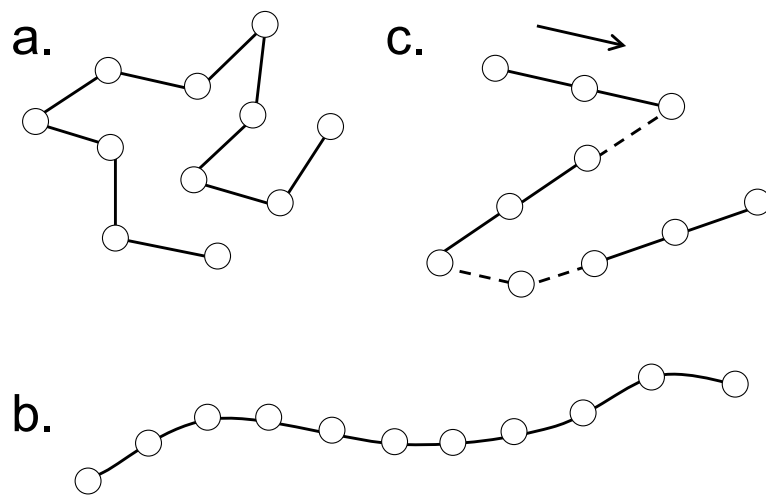


Figure 3

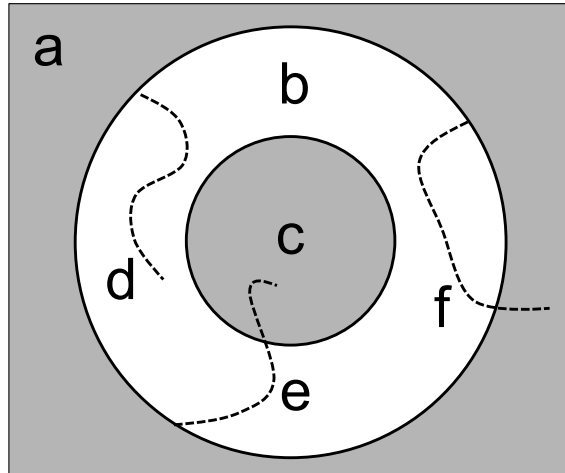


Figure 4

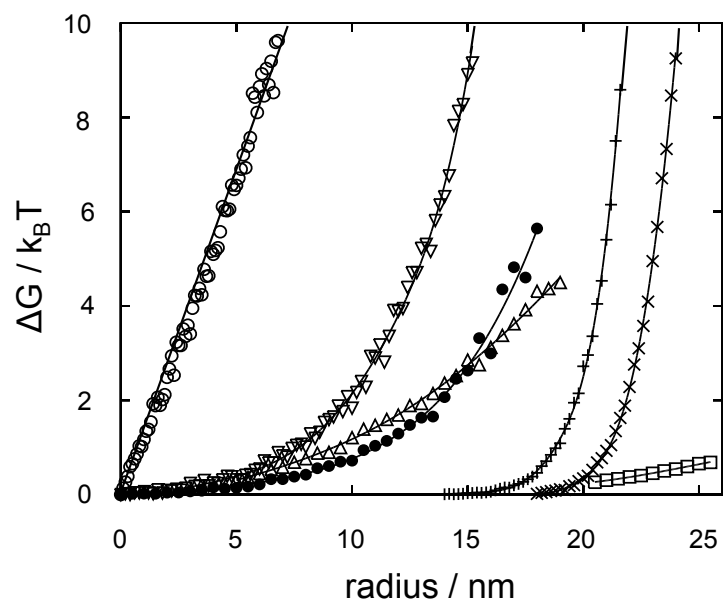
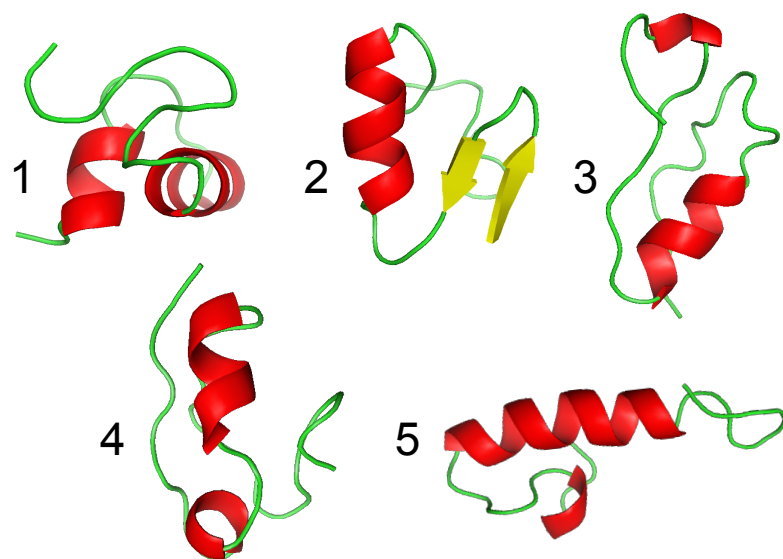


Figure 5



## References

- [1] R. Peters. Translocation through the nuclear pore complex: Selectivity and speed by reduction-of-dimensionality. *Traffic*, 6:421–427, 2005.
- [2] R. Lim, U. Aebi, and D. Stoffler. From the trap to the basket: Getting to the bottom of the nuclear pore complex. *Chromosoma*, 115:15–26, 2006.
- [3] G. Kabachinski and T.U. Schwartz. The nuclear pore complex structure and function at a glance. *Journal of Cell Science*, 128:423–429, 2015.
- [4] K.E. Knockenhauer and T.U. Schwartz. The nuclear pore complex as a flexible and dynamic gate. *Cell*, 164:0092–8674, 2016.
- [5] D. H. Lin and A. Hoelz. The structure of the nuclear pore complex (an update). *Annual review of biochemistry*, 88:725783, 2019.
- [6] M. P. Rout and G. Blobel. Isolation of the yeast nuclear pore complex. *Journal of Cell Biology*, 123:771–783, 1993.
- [7] O. Keminer and R. Peters. Permeability of single nuclear pores. *Biophys J.*, 77:217228, 1999.
- [8] H. Fischer, I. Polikarpov, and A.F. Craievich. Average protein density is a molecular-weight-dependent function. *Protein Sci.*, 13:28252828, 2004.
- [9] M. Eibauer, M. Pellanda, Y. Turgay, A. Dubrovsky, A. Wild, and O. Medalia. Structure and gating of the nuclear pore complex. *Nature Communications*, 6:2041–1723, 2015.

- [10] J. Kosinski, S. Mosalaganti, A. von Appen, R. Teimer, A.L. DiGuilio, W. Wan, K.H. Bui, W.J.H. Hagen, J.A.G. Briggs, J.S. Glavy, E. Hurt, and M. Beck. Molecular architecture of the inner ring scaffold of the human nuclear pore complex. *Science*, 352:363–365, 2016.
- [11] E. Ott, M.A. Jobst, C. Schoeler, H.E. Gaub, and M.A. Nash. Single-molecule force spectroscopy on polyproteins and receptorligand complexes: The current toolbox. *Journal of Structural Biology*, 197:3 – 12, 2017.
- [12] Y. Pang and R. Gordon. Optical trapping of a single protein. *Nano Letters*, 12:402–406, 2012.
- [13] L. Miao and K. Schulten. Transport-related structures and processes of the nuclear pore complex studied through molecular dynamics. *Structure*, 17:449459, 2009.
- [14] L. Miao and K. Schulten. Probing a structural model of the nuclear pore complex channel through molecular dynamics. *Biophysical Journal*, 98:1658 – 1667, 2010.
- [15] D. Ando and A. Gopinathan. Cooperative interactions between different classes of disordered proteins play a functional role in the nuclear pore complex of bakers yeast. *PLOS ONE*, 12:e0169455, 2017.
- [16] J.E. Kohn, I.S. Millett, J. Jacob, B. Zagrovic, T. M. Dillon, N. Cingel, R. S. Dothager, S. Seifert, P. Thiyagarajan, T. R. Sosnick, M. Z. Hasan, V. S. Pande, I. Ruczinski, S. Doniach, and K. W. Plaxco. Random-coil

- behavior and the dimensions of chemically unfolded proteins. *Proceedings of the National Academy of Sciences*, 101:12491–12496, 2004.
- [17] J.E. Kohn, I.S. Millett, J. Jacob, B. Zagrovic, T. M. Dillon, N. Cingel, R. S. Dothager, S. Seifert, P. Thiyagarajan, T. R. Sosnick, M. Z. Hasan, V. S. Pande, I. Ruczinski, S. Doniach, and K. W. Plaxco. Correction for kohn et al., random-coil behavior and the dimensions of chemically unfolded proteins, pnas 2004 101:12491-12496. *Proceedings of the National Academy of Sciences*, 102:14475–14475, 2005.
- [18] O. Kratky and G. Porod. Röntgenuntersuchung gelöster fadenmoleküle. *Rec. Trav. Chim. Pays-Bas.*, 68:11061123, 1949.
- [19] M. Doi and S.F. Edwards. *The Theory of Polymer Dynamics*. Clarendon Press, New York, 1986.
- [20] S. Choe and S.X. Suna. The elasticity of  $\alpha$ -helices. *J. Chem. Phys.*, 122:244912, 2005.
- [21] G.E.P. Box and M.E. Muller. A note on the generation of random normal deviates. *Ann. math. stat.*, 29:610–611, 1958.
- [22] A.D. Jenkins, P. Kratochvil, R.F.T. Stepto, and U.W. Suter. Glossary of basic terms in polymer science (iupac recommendations 1996). *Pure and Applied Chemistry*, 68:2287–2311, 1996.
- [23] P. Tompa and A. Fersht. *Structure and Function of Intrinsically Disordered Proteins*. CRC Press, Boca Raton FL, 2009.

- [24] N BenTal, D Sitkoff, I A Topol, A S Yang, S K Burt, and B Honig. Free energy of amide hydrogen bond formation in vacuum, in water, and in liquid alkane solution. *Journal of Physical Chemistry B*, 101(3):450–457, 1997.
- [25] Sheh-Yi Sheu, Dah-Yen Yang, H L Selzle, and E W Schlag. Energetics of hydrogen bonds in peptides. *Proceedings of the National Academy of Sciences of the United States of America*, 100(22):12683–12687, 2003.
- [26] D. E. Kim, D. Chivian, and D. Baker. Protein structure prediction and analysis using the rosetta server. *Nucleic Acids Research*, 32:W526–W531, 2004.
- [27] D. P. Klose, B. A. Wallace, and R. W. Janes. 2struc: the secondary structure server. *Bioinformatics*, 26:2624–2625, 2010.
- [28] H.-P. Hsu and P.K. Binder. Breakdown of the kratky-porod wormlike chain model for semiflexible polymers in two dimensions. *EPL*, 95:1–5, 2011.
- [29] B. Kobe. Autoinhibition by an internal nuclear localization signal revealed by the crystal structure of mammalian importin  $\alpha$ . *Nature Structural Biology*, 6:388–397, 1999.
- [30] G. Cingolani, C. Petosa, K. Weis, and C.W. Müller. Structure of importin- $\beta$  bound to the ibb domain of importin- $\alpha$ . *Nature*, 399:221–229, 1999.
- [31] B.M. Mandelbrot. *The fractal geometry of nature*. W.H. Freeman, 1982.